

MRI with its large field of view, excellent spontaneous vessel-tissue contrast, good spatial resolution, and functional approach to blood flow is very well adapted to visualization of cardiac as well as mediastinal structures, in contrast with echocardiography, which is limited by bone or air artifacts [1–15]. However, as for any “tomographic” technique, multiplanar MRI requires mental 3D reconstruction of cardiovascular anatomy from a series of sequential images 3–10 mm thick, obtained after processing.¹

A good knowledge of normal cardiac anatomy in the “useful” imaging planes usually performed (axial, coronal, sagittal, and guided according to the anatomical axis of the heart) is therefore an essential prerequisite. This approach allows segmental cardiovascular analysis² [16–20] by identifying the various cardiac chambers and great vessels, their location, and their mode of connection.

Healthy subjects with usual connections (SVC and IVC → RA → RV → PA and PV → LA → LV → Ao³) present a right–left arrangement of cardiac chambers which is correlated with the thoracic and abdominal arrangement. Due to the orientation of the anatomical axis of the heart, the “right” chambers are actually in a “right anterior” position compared to the “left” chambers, which are situated in a “left posterior” position (Figs. 2.1–2.3). Furthermore, due to crossover (twisting) of the great vessels at their origin, the pulmonary

artery and aorta do not comply with this right–left symmetry. At its origin, the ascending aorta (“left-sided” structure) is situated centrally and posteriorly (and to the right) of the pulmonary artery (“right-sided” structure), which is situated anteriorly (and to the left) (Figs. 2.1 and 2.4).

Many variants of position and cardiac and vascular connection (inversion) can be observed in congenital malformations. The various chambers (atria/ventricles) are therefore identified by morphological criteria as “morphologically right” (mRA, mRV) or “morphologically left” (mLA, mLV) regardless of their actual position (“right” or “left”).

After a general review of the principles of cardiovascular imaging and a few basic concepts, this chapter describes cardiovascular anatomy, illustrated by an atlas of normal imaging, which is completed by segmental sequential analysis (see Chap. 3).

2.1 General Principles

MRI examination, particularly in children, requires perfect sedation (or possibly even general anesthesia), as the slightest movement can significantly alter the image quality (see Chap. 1).

After a localizing sequence, the examination starts with axial spin-echo sequences, providing a precise and reliable three dimensional tomographic visualization of cardiovascular anatomy. On T1-weighted spin-echo-based sequences, the blood, circulating rapidly in vessels and cardiac chambers, usually generates spontaneous contrast (“low signal intensity” – black) compared to mediastinal fat (“high signal intensity” – white) and soft tissues (vessel walls and myocardium, “isosignal” – gray). Chambers and airways (lungs, trachea, etc.),

¹Real-time imaging is possible on more recent machines, which allows selection, on a beating heart image, of the most appropriate imaging plane to visualize the structure of interest.

²In the same way as for echocardiography, angiography or autopsy.

³SVC and IVC=superior vena cava and inferior vena cava, RA and LA=right and left atrium, RV and LV=right and left ventricle, PA=pulmonary artery and Ao=aorta.

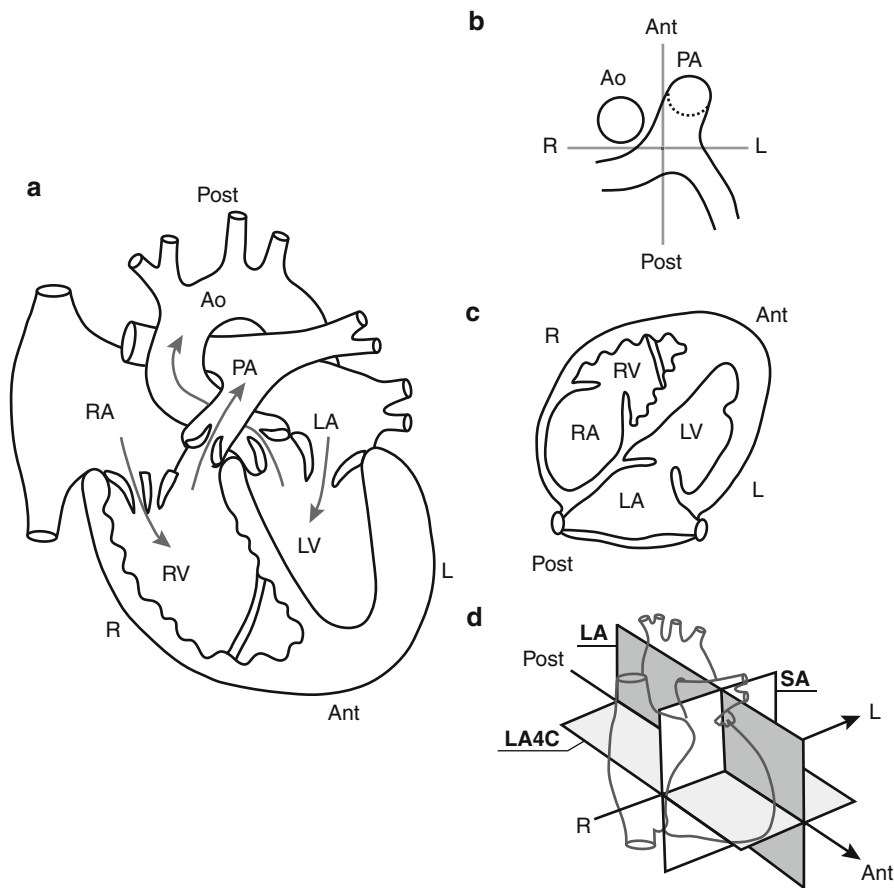


Fig. 2.1 Normal arrangement of cardiac chambers and great vessels. **(a)** Anatomical diagram, **(b)** Section through the origin of the aorta (Ao) and pulmonary artery (PA), **(c)** “Four-chamber” axial image. **(d)** Diagram of the arrangement of the cardiac chambers in the thorax. **(a)** The aorta (Ao) emerges from the (morphologically) left ventricle (LV-mLV), and the pulmonary artery (PA) emerges from the (morphologically) right ventricle (RV-mRV). **(b)** At its origin, the ascending aorta is in a central

position, posteriorly and to the right of the pulmonary artery, which is situated anteriorly and to the left. **(c, d)** “Right” chambers are “right anterior” and “left” chambers are “left posterior” (also see Figs. 2.2 (anatomical axis) and 2.4 (short-axis and long-axis images) and Figs. 2.4, 2.6, and 2.7 (“four-chamber” axial images). Right atrium (RA) and left atrium (LA). Note that the loop rule indicating that both the Ao and mRV are situated on the same side applies here (see below)

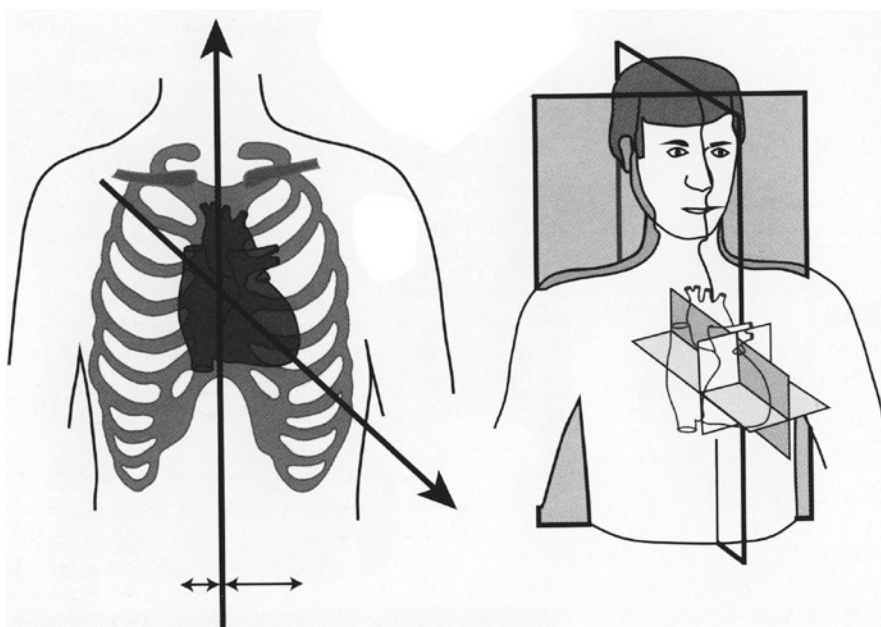
bone and calcifications also appear black (see Chap. 1). The field of view is adapted to the child’s thorax including the heart, mediastinum, lungs, and extends into the neck or even the abdomen to analyze the position of abdominal viscera.

2.2 Choice of Imaging Planes

Although acquisition of a first series of axial images is essential, the choice of the other imaging planes (the most appropriate: other axial series, coronal, sagittal,

and/or oblique series) cannot be standardized. The examination protocol is adapted to each individual case by referring to the clinical file and the problems not resolved by echocardiography, and also the information gradually obtained during acquisition of MR sequences. The use of oblique slices containing vascular structures (situated away from the heart) is sometimes very useful, as these structures are not always clearly visualized on echocardiography. The limiting factor when elaborating this examination protocol (as is often the case in imaging) is the duration of the examination. The use of rectangular fields of view with asymmetrical matrices (e.g., 96×256) and several

Fig. 2.2 Anatomical axis of the heart. The anatomical axis of the heart or long-axis (base-apex) is usually directed anteriorly, inferiorly, and to the left. Consequently, the atria are situated posteriorly and superiorly, and the ventricles are situated anteriorly and inferiorly (see text and Figs. 2.1c and 2.5c)



excitations (at least 4) reduces the examination time and movement artifacts [21, 22]. Under these conditions, the acquisition time of a conventional spin-echo (SE) sequence is in the range of 2–4 min (series of 5 images in a given imaging plane). Fast imaging sequences have strongly reduced imaging time down to a few seconds allowing breath-hold acquisition.⁴ However, the total examination time for a thorough examination comprising a series of 6–10 sequences is around 30–45 min. This procedure is well tolerated even by very young, sick, or premature patients.

To improve visualization of small vessels, we recommend two series of thin (3–5 mm), intertwined, and overlapping (2–3 mm) slices in each plane of interest.

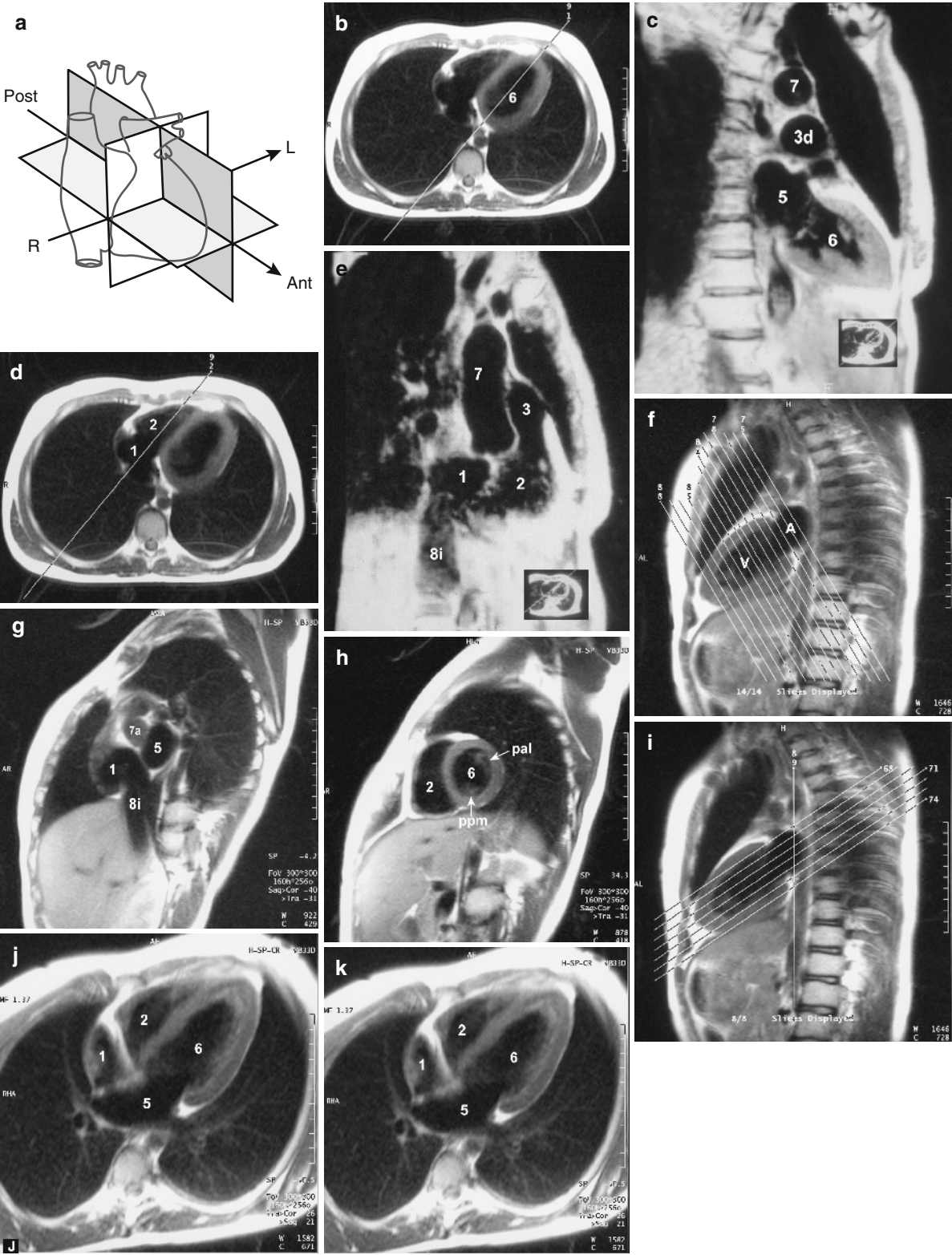
2.3 Study of Blood Flow

MR study of blood flow is based on two techniques: black-blood imaging and bright-blood imaging (see Chap. 1).

2.3.1 Black-Blood Imaging

The spin-echo sequence (historically, the first imaging sequence to be developed) is currently the most commonly used black-blood technique for cardiac imaging. Due to long acquisition times, black blood fast spin-echo sequences have replaced traditional spin-echo sequences. In black blood fast spin-echo sequences circulating blood is generally black (as blood flows out of the slice and due to spin dephasing [23–30]). The images obtained are excellent for anatomical delineation generating “spontaneous” contrast between circulating blood which is black and soft tissues (and thrombus) which are gray (fat appears white). However, when blood circulates slowly (venous flow or end-diastole arterial flow as, for example, in aortic aneurysm or false lumen), flow effects may be confusing. An intermediate intravascular signal or even a high signal intensity due to inflowing unsaturated blood can be observed and may be mistaken for obstruction or thrombus [31]. This situation can be clarified by using sequences with saturation bands outside the Fov of interest [24, 30] (which restore the usual contrast between black circulating blood and gray thrombus) or bright-blood imaging (circulating blood is white and thrombus is gray), which is briefly discussed later [25–36].

⁴Not always possible in practice in very young patients – feasible in elderly cooperative children and adults.



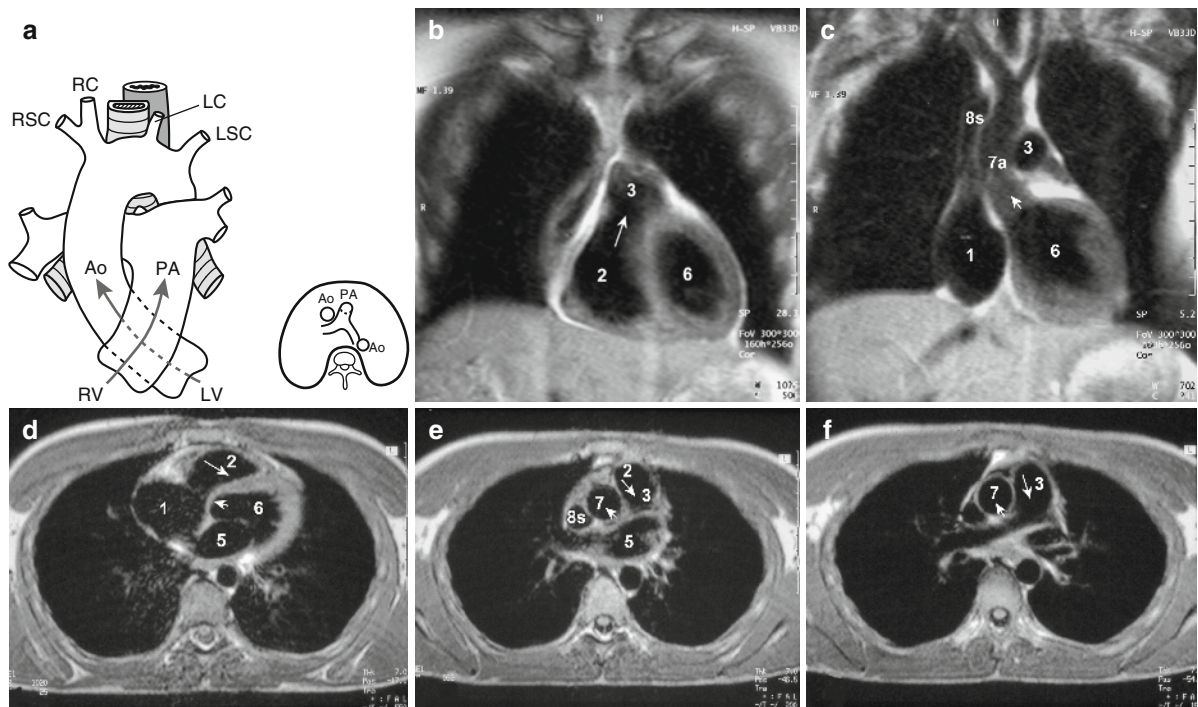


Fig. 2.4 Crossover (Twisting) of the aorta (Ao) and pulmonary artery trunk (PA) at their origin. Schematic diagram (a) and coronal *fast spin-echo* images through the origin of the pulmonary artery (long arrow, 3 – b) and the aorta (short arrow, 7 – c). Axial *fast spin-echo* images through the origin of the aorta (d) and pulmonary artery (e, f). The ascending aorta (Ao-7) at its

origin is in a central position, posteriorly and to the right of the pulmonary artery (PA-3) which is situated anteriorly and to the left. The vessels cross over at their origin (*short and long arrows*): the *pulmonary artery* emerges from the right ventricle (2) and the *aorta* emerges from the left ventricle (6); right atrium (1), superior vena cava (8s)

Incomplete blood signal suppression and respiratory motion artifacts are also potential limitations of fast spin-echo sequences. Respiratory motion algorithm or navigator echo techniques using diaphragmatic motion have hence been proposed. A double inversion pulse can be added at the beginning of the sequence for blood pool signal suppression and optimization of black blood imaging [37]. Single slice or better multislice double IR T2 weighted sequences

allowing excellent image quality during one breath-hold⁴ [38]) are now becoming the gold standard for black blood imaging and are used routinely, replacing fast spin-echo sequences. Black blood sequences should be performed before gadolinium injection as the latter impairs proper blood suppression by the IR pulse.

Fig. 2.3 Images in the anatomical axis of the heart. (a) Schematic diagram. (b–g) Long-axis *two-chamber* (vertical dark gray plane) and *four-chamber* (true four-chamber image – horizontal light gray plane) and short-axis *two-chamber* images. The “left chamber” long-axis images (c) and “right chamber” long-axis images (e) were obtained from the axial image (“four-chamber”), by placing the imaging planes in the anatomical axis of the heart on the left (b) and right (d) chambers, respectively. Short-axis images (double oblique *true short-axis*) are obtained from the long-axis image (f), by placing the

imaging planes perpendicular to the anatomical axis of the heart: posterior images through the atria (g) and anterior images through the ventricles (h). (j, k) Four-chamber axial images in the anatomical axis of the heart (*true four-chamber image*), obtained from the long-axis image (f) by placing imaging planes parallel to the anatomical axis of the heart; right atrium (1), right ventricle (2), left atrium (5), left ventricle (6), ascending aorta (7), inferior vena cava (8i), anterolateral papillary muscles (pal), and posteromedian papillary muscles (ppm)

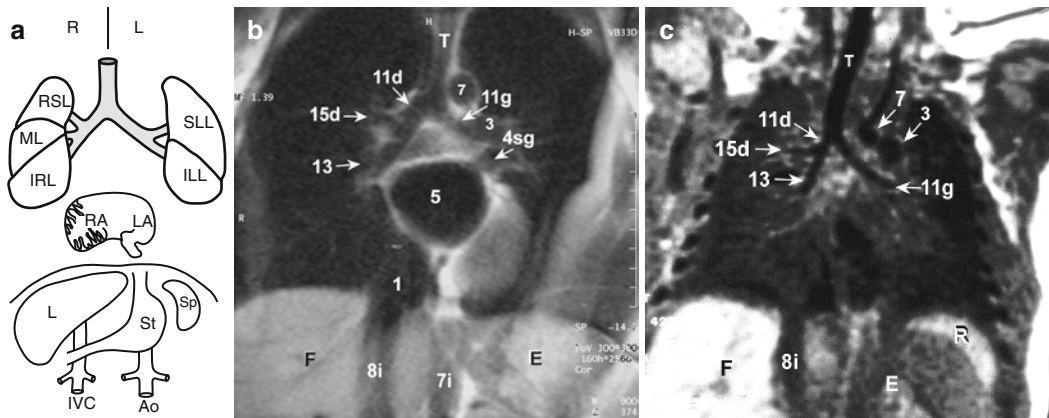
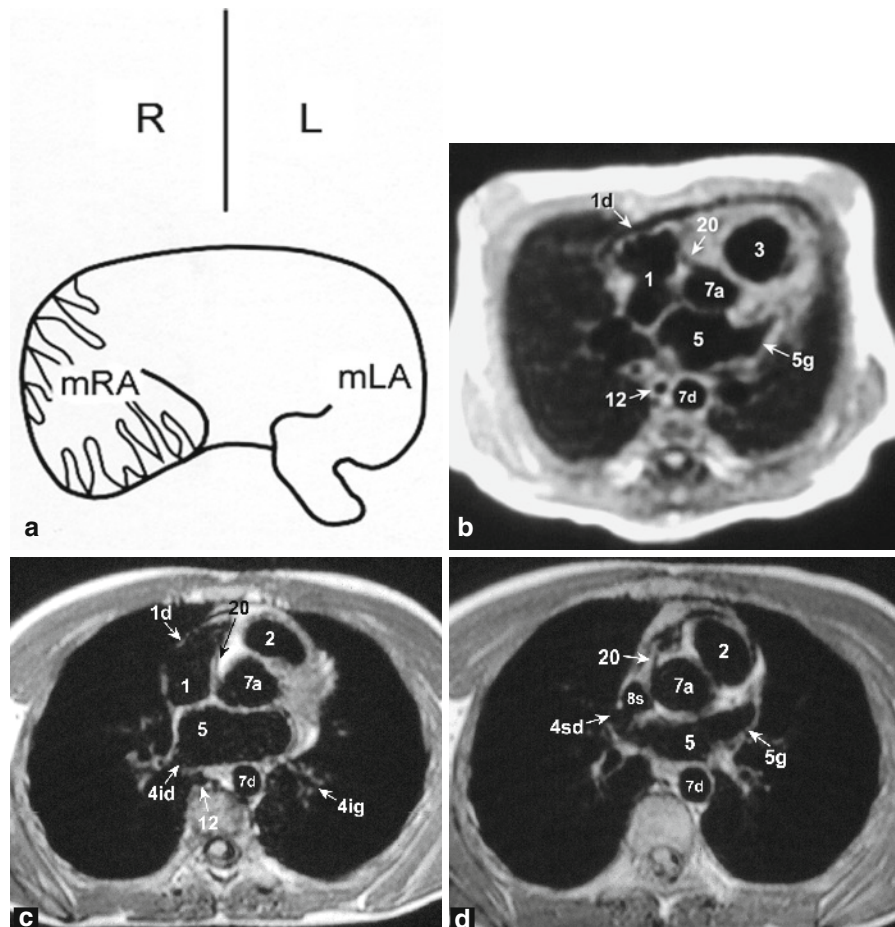


Fig. 2.5 Correlation between the atrial, thoracic, and abdominal arrangements in situs solitus (normal atrial position). (a) Schematic diagram. (b, c) Coronal spin-echo images in a child (b) and an infant (c). Right-left pulmonary asymmetry: right main bronchus (11d) on the right and left main bronchus (11g) on the left correlated with the atrial positions; right atrium (RA-1) on the right and left atrium on the left (LA-5). The same applies to the position of abdominal organs: Liver (L) on the

right and spleen (Sp) and stomach (St) on the left, inferior vena cava (IVC-8i) on the right and abdominal aorta (Ao-7i) on the left. Right upper lobe (RUL), left upper lobe (LUL), middle lobe (ML), right lower lobe (RLL), left lower lobe (LLL); pulmonary artery (left-3), left superior pulmonary vein (4sg), ascending aorta (7a), left main bronchus (11g), bronchus intermedius (13), right upper lobe bronchus (15d) (also see Chap. 3, Figs 3.2 and 3.19b and Chap. 5, Fig. 5.23)

Fig. 2.6 “Morphologically” right atrium (mRA) and “morphologically” left atrium (mLA). (a) Schematic diagram. (b) Axial images in an infant. (c, d) Axial images in a young adult. The “morphologically” right atrial appendage (1d) has a triangular shape with a broad implantation on the right atrium (1) (situated on the right) which is connected to the superior vena cava (1). The “morphologically” left atrial appendage (5g) has a finger-like shape with a narrow implantation on the left atrium (5) (situated on the left); pulmonary infundibulum (2i) below the pulmonary artery, right superior (4sd), right inferior (4id), and left inferior (4ig) pulmonary veins, ascending and descending aorta (7 and 7d), superior vena cava (8s); note the origin of the right coronary artery (20) (also see Chap. 3, Fig. 3.19b)



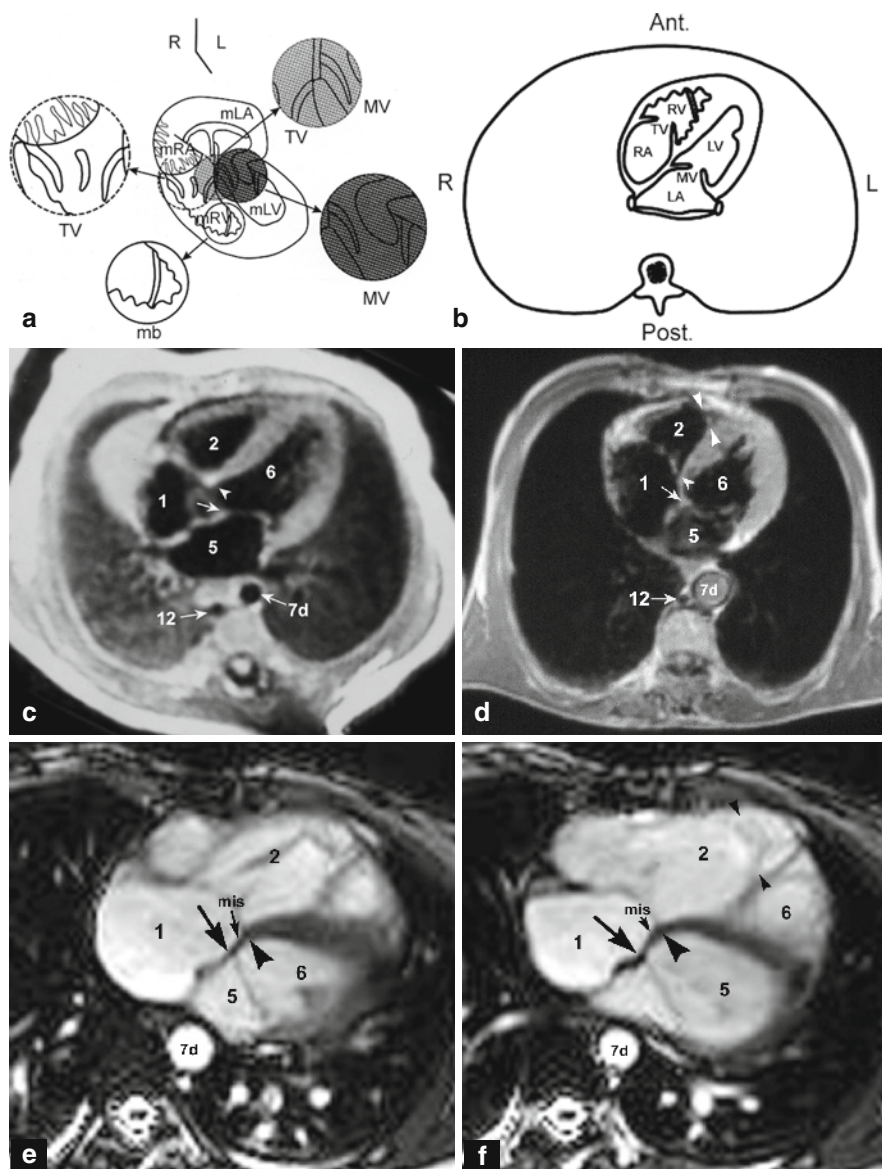


Fig. 2.7 “Morphologically” right ventricle (mRV) and “morphologically” left ventricle (mLV). (a) Schematic diagram. (b) “Four-chamber” axial spin-echo images through the ventricular chambers in an (c) and an adolescent (d). Gradient-echo cine-MR axial images (e and f). Morphologically right atrium (mRA) and left atrium (mLA). Identification of mRV and mLV is based on the insertion of the atrioventricular valve leaflets in relation to the interventricular septum: the tricuspid valve (TV—arrowhead—not VM) which always opens into an mRV, is always situated more anteriorly (and inferiorly

to the apex of the heart) compared to the mitral valve (MV—arrow), which always opens into an mLV and which is situated more posteriorly. This offset of the valves delineates the membranous interventricular septum (mis). The mRV is also identified (second criterion) by the presence of trabeculations and the moderator band (between arrow heads); right atrium (1) and left atrium (5), right ventricle (2) and left ventricle (6), descending aorta (7d), azygos vein (12) (also see Chap. 3, Figs. 3.17c and d, 3.19c, 3.20e, 3.21b, and 3.24d and Chap. 7, Fig. 7.14 and Chap. 8, Figs. 8.14 and 8.22)

2.3.2 Bright-Blood Imaging

Bright-blood imaging techniques give physiologic information on blood flow. Bright-blood imaging uses gradient-echo (GE) sequences with flow compensation

(circulating flow-white and soft tissues-dark gray). The acquisition time is sufficiently short to allow breath-hold images⁴ [25–27]. They provide dynamic ECG-gated cine-MRI images [25–27, 33–36, 39, 40], or MR angiography images [28–31] on which soft tissues are

almost completely suppressed by saturation and/or by special algorithms such as Maximum Intensity Projection (MIP). This imaging therefore allows a dynamic approach to normal flow (bright-blood) and a semi-quantitative approach to abnormal flow (black flow void *jets* in stenoses, shunts, and regurgitations) [33–36] (see Chap. 1).

It is also possible to obtain flow quantification (velocity mapping) by using specific sequences (phase-contrast MR angiography) (see Chap. 1) [40–48].

Recently introduced Balanced-SSFP (Fiesta/GE, True-FISP/Siemens, Balanced-FFE/Philips) [49] sequences generate excellent, strongly flow-enhanced cine-MR images not relying on inflow effects. They are now used routinely in place of traditional GE cine-MRI and for anatomical cardiovascular analysis, as a complement to black-blood images, whenever the latter are inconclusive. Contrary to black-blood sequences, they can be performed not only before but also after gadolinium administration (see Chap. 1).

Contrast-enhanced gradient-echo images (CE-MR angiography) using intravascular Gadolinium administration can also be obtained displaying 3D luminal information on a large Fov (see Chap. 1).

2.4 Segmental Analysis of Cardiac Anatomy

Segmental analysis of cardiac anatomy (see Figs. 2.4–2.7; atlas and Chap. 3, Fig. 3.17) [16] and vascular connections is performed by carefully selecting the orientation of slices on axial, coronal, or sagittal planes, as well as oblique planes, according to the anatomical axes of the heart or vessels studied (aorta, pulmonary artery, vena cava, or pulmonary vein, surgical procedures, etc.).

Axial images (generally performed first) (atlas Figs. A) define the position of the ascending aorta, which is “normally” in a “central” situation posteriorly and to the right of the pulmonary artery (which is situated anteriorly and to the left) (A6), identify the “morphologically” right and left atria and ventricles (A10–12), evaluate the caliber of branches of the pulmonary artery (A4–6), and identify pulmonary veins “normally” converging onto the left atrium (A7, 8, and F10).

Coronal images (atlas Figs. F) more clearly visualize the superior vena cava and inferior vena cava normally draining into the right atrium (F7, 10), the left ventricle and its outflow tract giving rise to the ascending aorta, and the trachea and the main bronchi (bronchial arrangement, Fig. 2.5 and atlas F11). Posterior images show the left atrium (F10, 11) and descending aorta, and anterior images show the right ventricle with the origin of the pulmonary artery.

Sagittal images (Atlas Fig. S) are well adapted to the study of all of the right ventricular outflow tract (ventricle, infundibulum and pulmonary artery trunk) (S3–5), as well as the trachea (S2).

“Short-axis” two-chamber and “long-axis” two-chamber and four-chamber images (Fig. 2.3) respecting the right–left symmetry clearly distinguish the right chambers from the left chambers [50] (the right atrium is identified by drainage of the venae cavae). They can be used to confirm transposition of the great vessels or a ventricular or atrial septal defect.

Sagittal oblique images (equivalent to “LAO”) (Fig. 2.8) are essential to study the aortic arch.

2.5 Normal Cardiovascular Anatomy

Identification of the numerous pathological variants, particularly in the context of congenital heart disease, requires a perfect knowledge of normal anatomy. Although some paired organs have a “symmetrical” arrangement (cerebral hemispheres, kidneys, etc), other paired organs are not symmetrical (lungs, bronchial tree, branches of the pulmonary artery, atria, and ventricles). Some “asymmetrical” viscera and vessels are also clearly lateralized to the right (liver, inferior vena cava), while others are lateralized to the left (stomach, spleen, abdominal aorta, and heart) (Fig. 2.5). Determination of the disposition or situs of asymmetrical atrial, pulmonary [18], and abdominal structures [19] (normal position: situs solitus – Figs. 2.5, 2.6, 2.7, and 2.9) is important in congenital heart disease, as some malformations are associated with situs anomalies.

The anatomical axis of the heart (base-apex long-axis) is usually directed anteriorly, inferiorly, and to the left, and not according to one of the conventional orthogonal axes (right-left, superior-inferior, anterior-posterior) (Fig. 2.2 and see Chap. 3,

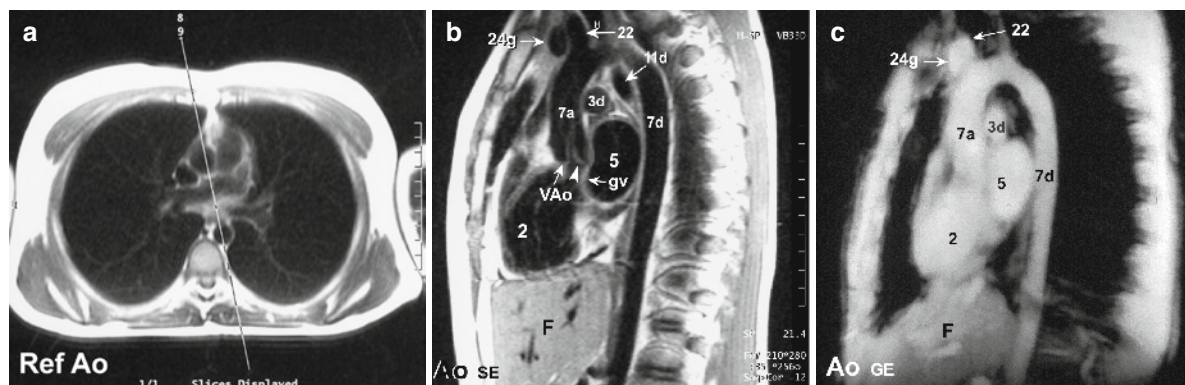


Fig. 2.8 Imaging plane (a) to obtain a LAO image containing the aortic arch. Spin-echo black-blood image (b) and gradient-echo bright-blood (c) images. The aortic valve (AoV) is clearly visualized (the posterior leaflet is continuous with the anterior

leaflet of the mitral valve) (Fig 2.8 and see Chap. 2 3, Fig. 6.22c). Ascending and descending thoracic aorta (7a and 7d), right pulmonary artery (3d), left atrium (5), right ventricle (2), left brachiocephalic vein (24g), right main bronchus (11d)

Sect. 3.2.4.1.7).⁵ Consequently, the atria are situated posteriorly and superiorly, and the ventricles are situated anteriorly and inferiorly (the right chambers are actually right anterior and the left chambers are left anterior); hence, the value of so-called “long-axis” two-chamber and four-chamber images is parallel to the anatomical axis of the heart, and “short-axis” two-chamber images are perpendicular to this axis [50] (Fig. 2.5).

Compared to conventional orthogonal planes,⁶ the cardiac mass is therefore not arranged symmetrically: the left atrium is the posteriormost chamber (anterior to the spine), the right ventricle is the anteriormost chamber (posterior to the sternum), the right atrium is the chamber situated mostly to the right and the left ventricle is the chamber situated mostly to the left. This particular arrangement is clearly visualized on axial images (particularly on the so-called “four-chamber” image – Fig. 2.1 and atlas A10–12) and is also observed on coronal (right atrium to the right and left ventricle to the left) (atlas F4–7) and sagittal images (right ventricle anteriorly and left atrium posteriorly) (atlas S2–5).

Cardiac chambers also have specific morphological features corresponding to well-defined criteria. In Chap. 3, we shall see that a chamber considered

to be strictly normal anatomically can occupy an abnormal situation; the same applies to the great vessels.

The differentiation of “right-sided” structures from “left-sided” structures is further complicated by twisting of the great vessels at their origin: the aorta, which emerges from the left ventricle, belongs to the systemic or “left” circuit, but is actually situated on the right and posteriorly to the pulmonary artery which belongs to the pulmonary or “right” circuit (“right-sided” structure situated on the left and anteriorly) – Figs. 2.1 and 2.4; atlas A6).

After a brief description of the anatomy of each structure, the MR criteria for recognition of “morphologically” right and left chambers and the distinction between aorta and pulmonary artery are described.

2.6 MR Segmental Cardiovascular Anatomy

2.6.1 “Morphologically” Right Atrium (mRA)

The right atrium, normally situated to the right and posteriorly, is divided into a venous component, vestibule, septum, and atrial appendage. The venous component normally receives the superior vena cava superiorly (into which merge the right and left brachiocephalic veins) and the inferior vena cava

⁵ It is more “horizontal” in newborn infants compared to adults, where it is more vertical.

⁶ Axial, coronal, and sagittal.

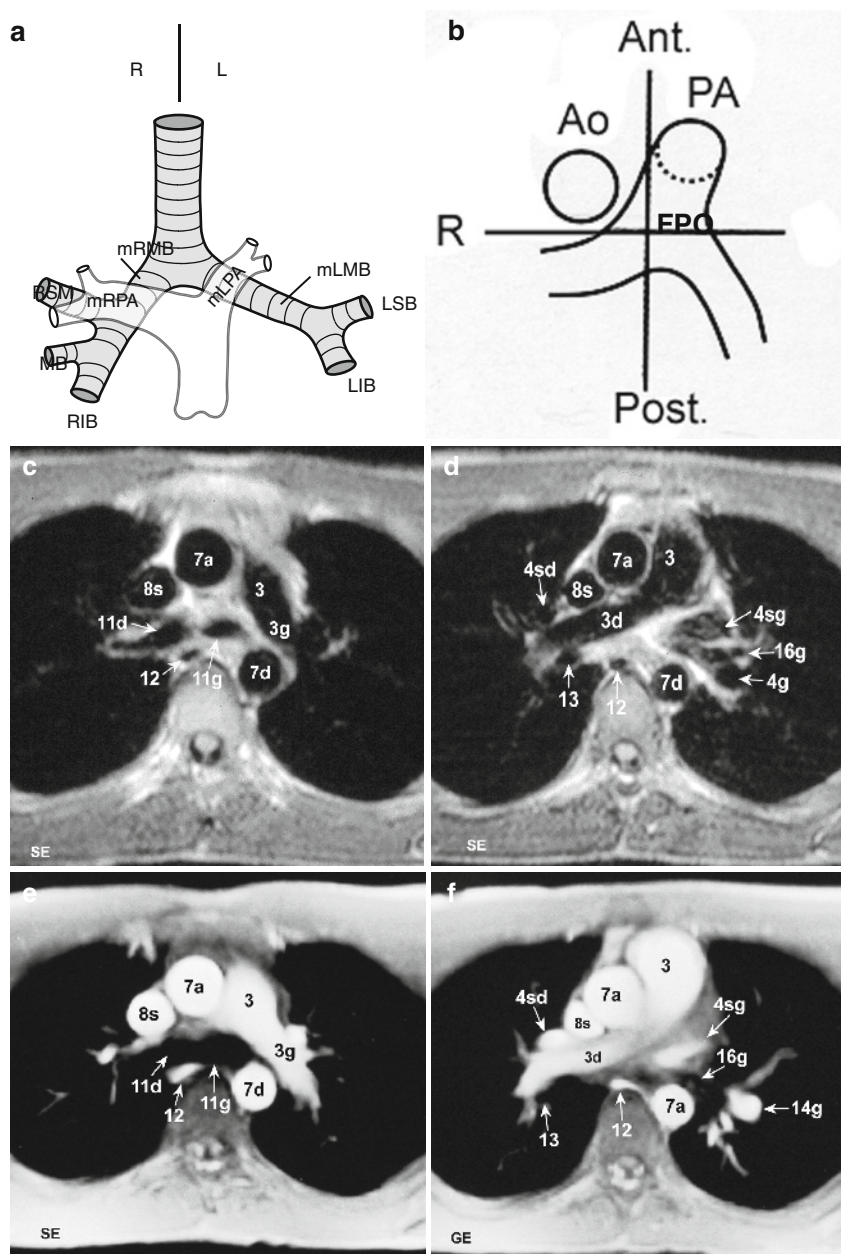


Fig. 2.9 Right and left pulmonary artery and bronchial arrangement. Schematic diagram (a) and section (b). The right (mRPA) and left (mLPA) pulmonary arteries, right (mRMB) and left (mLMB) main bronchus, right (RULB) and left (LULB) upper lobe bronchus, right middle lobe bronchus (RMLB), right (RLLB) and left (LLL) lower lobe bronchus, aorta (Ao), and pulmonary artery (PA). MR axial images through the right (d and f) and left pulmonary arteries (c and e). (c, d) Anatomical spin-echo black-blood images. (e, f) Gradient-echo bright-blood images. At its origin, the aorta (7) is situated anteriorly and to the right of the pulmonary artery (3). The pulmonary artery divides into a long, large right branch situated in a “coronal” (oblique) plane (a, b and 3d d, f, atlas F8) and a shorter left branch continuous with the trunk situated in a “sagittal” (oblique) plane (a, b and 3g, c, e, atlas S4). Vascular structures appear white on gradient-echo sequences, allowing

vessels to be distinguished from bronchial structures in the hila (atlas A4, A6). This right–left pulmonary artery arrangement is correlated with the tracheobronchial arrangement, i.e., short, vertical, and eparterial right main bronchus (tri-lobed lung) and long, horizontal, and hyparterial left main bronchus (bilobed lung) (diagram). As described in Chap. 3, the thoracic arrangement is used to establish the atrial arrangement or atrial situs (Fig. 2.5b, c, atlas F11 and see Chap. 3, Figs. 3.1, 3.2, 3.4 and 3.7 and Chap. 5, Figs. 5.23 and 5.24). Pulmonary artery (3), right branch (3d) and left branch (3g), ascending and descending thoracic aorta (7a and 7d), left and right superior pulmonary veins (4sd and 4sg), superior vena cava (8s), left and right main bronchus (11d and 11g), bronchus intermedius (13), left lower lobe artery (14), left lower lobe bronchus (16g). *Eparterial: parallel and posterior to the pulmonary artery **Hyparterial: crossing underneath the pulmonary artery

inferiorly (which receives the hepatic veins) and the coronary sinus (close to the septum). The inferior vena cava has a valve (Eustachian valve of the inferior vena cava). The coronary sinus also has a valve (Thebesian valve of the coronary sinus). The crista terminalis is a vertical structure in the prolongation of the Eustachian valve, which separates the venous component from the appendage (Fig. 2.11a, c). All of the pectinate muscles, arising from the crista terminalis, converge onto the right atrial appendage. Filamentous structures attached to the crista terminalis are consistent with a Chiari's network *reseau* (arrows), embryological remains of no pathological significance (Fig. 2.10).

The triangular right atrial appendage has a large implantation base superiorly, laterally, and anteriorly

to the venous component (Fig. 2.6, atlas A7 and see Chap. 3, Figs. 3.19b et 3.24d).

The criteria for identification of the right atrium are:

- Broad triangular shape of the atrial appendage (Fig. 2.6, atlas A7 and see Chap. 3, Figs. 3.19b and 3.24c)
- Connection to the superior vena cava and especially the inferior vena cava (more reliable criterion) (Atlas F7, 10, S1, and Fig. 2.3 short-axis);
- The presence of a crista terminalis on axial MR images (arrows, Fig. 2.11a and c) is a feature that is of particular value to identify the mRA in anomalies of position of the heart such as Dextrocardia (Chap. 3, Fig. 3.28).

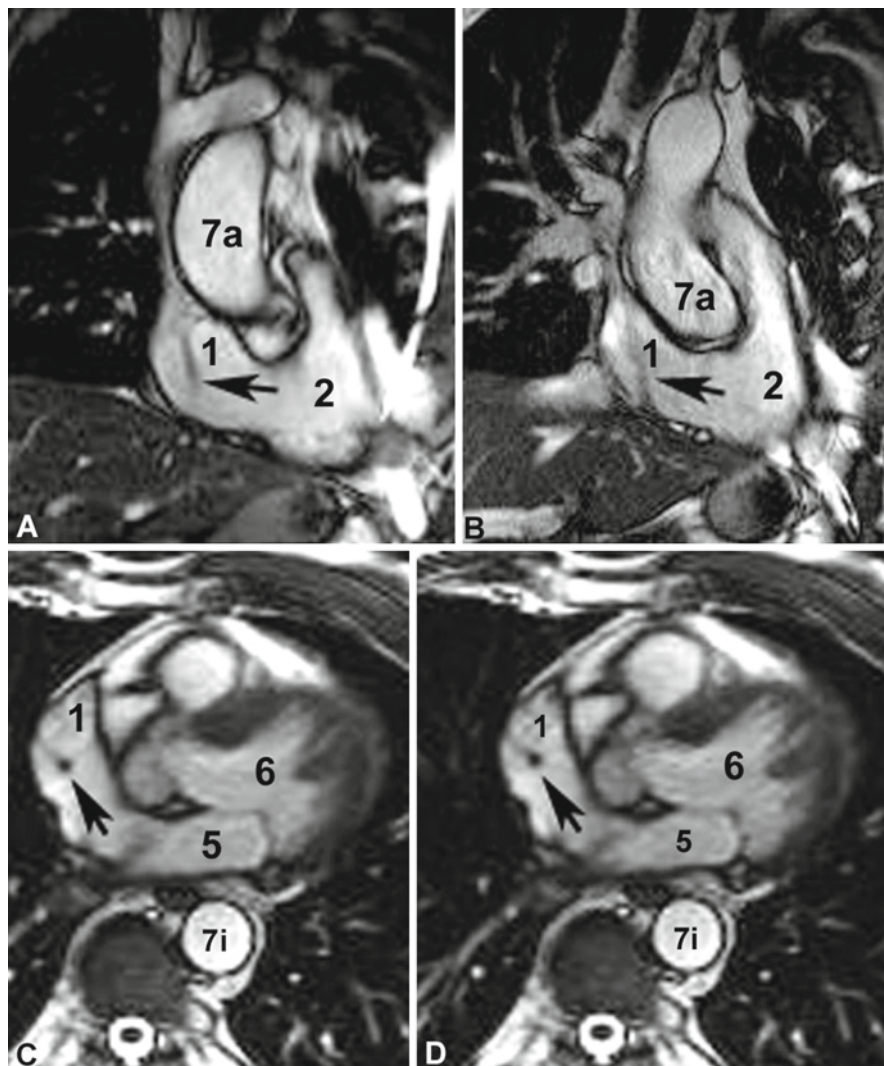
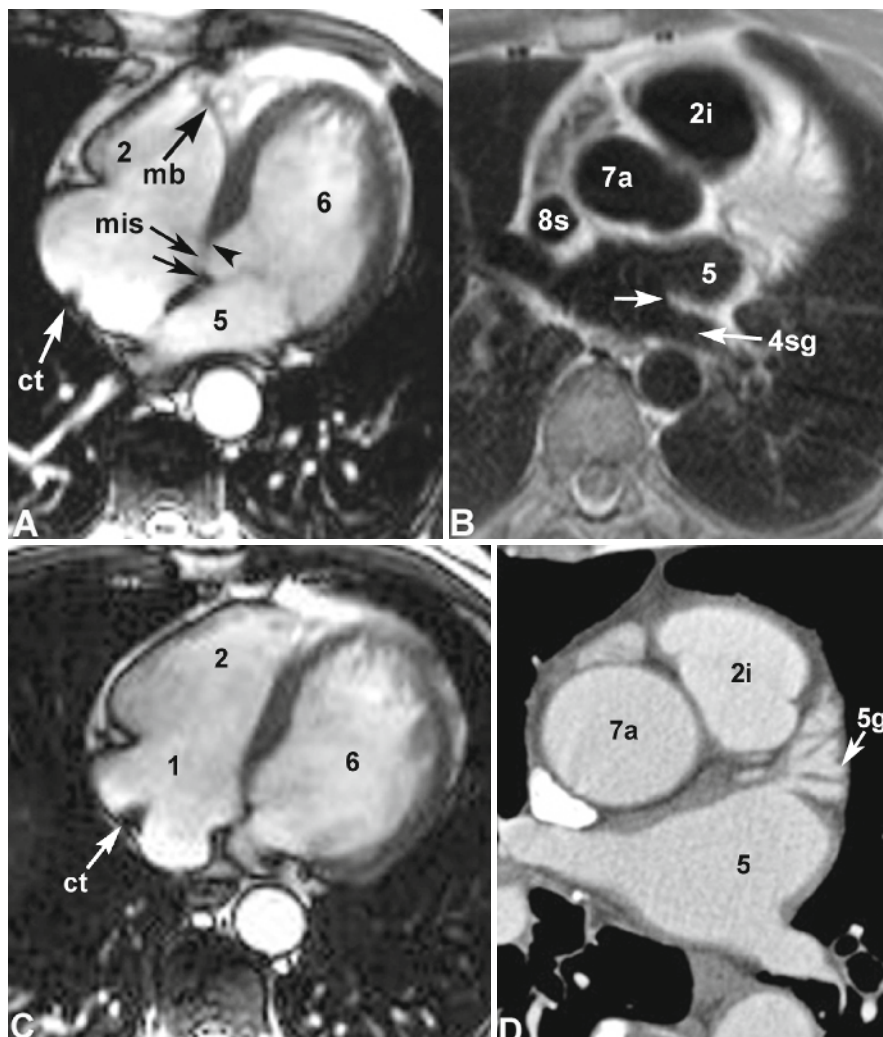


Fig. 2.10 Coronal (a and b), and axial (c and d) gradient-echo images. The presence of posterior filamentous structures attached to the crista terminalis is consistent with a Chiari's network, (arrows), embryological remains of no pathological significance

Fig. 2.11 Axial gradient-echo (a and c), spin-echo (b), and CT (d) images. Small heart anatomical and physiological structures to be remembered: The moderator band (mb A) which extends anteriorly from the main papillary muscle on the anterior wall to the interventricular septum; the vertical structure of the crista terminalis (CT ct, on images a and c) in the prolongation of the Eustachian valve, separating the venous component from the appendage of the right atrium (the presence of the crista terminalis is also a feature which is of particular value to identify the mRA in anomalies of position of the heart (see Chap. 3, Fig. 3.28)); the fibrous spur (arrow b) separating the left appendage and the abutting superior left pulmonary vein (4sg); the offset of the mitral (arrowhead) and tricuspid (arrow) valves, which delineates the membranous interventricular septum, (mis) is also visible (a); pectinate muscles within the left atrial appendage (5g) which are well seen on this CT image with an excellent spatial resolution (d). Right atrium (1), left atrium (5), right ventricle (2), left ventricle (6), descending aorta (7d)



2.6.2 “Morphologically” Left Atrium (mLA)

The left atrium, normally situated posteriorly and to the left, is also divided into a venous component, vestibule, septum, and atrial appendage. The smooth-walled venous component normally receives the four (or more) pulmonary veins. The valve of fossa ovalis largely covers the superior part of the septum secundum, even ensuring, in the absence of fusion of these two structures, a watertight shunt-free seal between the atria, provided the pressure in the left atrium exceeds that in the right atrium, as a patent foramen ovale is detected in one-third of the general population [17]. The pectinate muscles, less well developed than on the right, are almost exclusively situated in the atrial appendage (Fig. 2.11d). The morphology of the

left atrial appendage is also very different from that of the right atrial appendage. It has a hooked finger-like shape with a narrow connection to the atrium (Fig. 2.6, atlas A7 and F6, 7 and see Chap. 3, Fig. 3.16).

The criteria for identification of the left atrium are therefore:

- Narrow finger-like atrial appendage (Fig. 2.6, atlas A7 and see Chap. 3, Fig. 3.16)
- Connection to the pulmonary vein (less reliable criterion) (atlas F8–10, A7 and 8).

N.B.: the criteria for identification of the atria based on morphological differences between the right atrial appendage and left atrial appendage are not always obvious on MR or echocardiographic imaging. The venous connections are also not an absolute criterion. Chapter 3 describes in more detail other more reliable

criteria that are more readily accessible on MRI for determination of atrial situs (bronchial arrangement, see Fig. 2.5, Chap. 3).

2.6.3 “Morphologically” Right Ventricle (mRV)

The right ventricle (Fig. 2.7), normally situated anteriorly and to the right, has a triangular pyramid shape, composed of three walls: anterior (sternocostal), inferior (diaphragmatic), and medial, convex towards the right ventricle (interventricular septum). The base of the right ventricle corresponds to the tricuspid valve and, more anteriorly to the left, the pulmonary valve, which covers the subpulmonary conus arteriosus or infundibulum (myocardial tube separating the semilunar and atrioventricular valves). It comprises an entry chamber (compartment), an apex (containing many coarse trabeculations), and an ejection chamber (arterial compartment corresponding to the muscular infundibulum). The tricuspid valve⁷ opens into the right ventricle. It is composed of three triangular leaflets: anterior, inferior, and medial or septal, corresponding to the three walls. The insertion of one of the leaflets in relation to the interventricular septum is characteristic of the tricuspid valve. The tricuspid valve is always situated more anteriorly (and inferiorly towards the apex of the heart) compared to the mitral valve (which is situated more posteriorly, offset of the valves) (Fig. 2.7 and atlas A9, 10 – also see Chap. 3, Figs. 3.17c and d, 3.19c, 3.20e, 3.21b and 3.24d).

This offset of the valves delineates the membranous interventricular septum⁸ (mis) Fig. 2.7 and atlas A10). The right ventricle presents many trabeculations corresponding to papillary muscles; the moderator band (septomarginal trabecula) extends from the main papillary muscle on the anterior wall to the interventricular septum, anteriorly and below the infundibulum (Atlas A9, 10).

Criteria for identification of the right ventricle are therefore:

- The tricuspid valve which always opens into a right ventricle; it is identified by its more anterior septal insertion compared to that of the mitral valve (offset

of the valves depicted on “four-chamber long-axis” image and axial images (Fig. 2.7 and Atlas A9, 10)).

- The presence of a muscular subpulmonary infundibulum (conus) (atlas, sagittal images – long-axis images Fig. 2.3e), situated between the pulmonary valve and the tricuspid valve (space between the tricuspid and pulmonary rings) (see axial image, atlas A8, 9 through the pulmonary infundibulum).
- The presence of coarse trabeculations and the moderator band, generally clearly visible on axial images (atlas A9, 10).

2.6.4 “Morphologically” Left Ventricle (mLV)

The left ventricle (Fig. 2.7), normally situated to the left and anteriorly, has a truncated conical ellipsoid shape (bullet shape) and its myocardium is normally much thicker than that of the right ventricle.⁹ It has two externally convex walls, the right septal wall (the posterior two-thirds correspond to the smooth interventricular septum) and the free left wall, which is less trabeculated than the right endocardial surface. The base is entirely occupied by the mitral and aortic rings, which are continuous. Like the right ventricle, the left ventricle comprises an entry chamber (atrial compartment), an apex (containing fine trabeculations), and an ejection chamber. The mitral valve,¹⁰ opens into the left ventricle. Also known as the bicuspid valve, it is composed of two quadrilateral leaflets (or cups), the anterior leaflet and the posterior leaflet, with no insertion on the interventricular septum. There is a “mitro-aortic” continuity between the posterior part of the aortic root (posterior aortic leaflet) and the anterior leaflet of the mitral valve (Fig. 2.8 and see Chap. 2, Fig. 22c). The absence of insertion of the mitral valve onto the septum and the presence of two papillary muscles (anterolateral and posteromedian) on the free wall are characteristic of the left ventricle. The mitral valve is always situated posteriorly compared to the tricuspid valve (offset of the valves) (Fig. 2.7 and atlas A9 and 10).

⁷Strictly speaking, according to the new nomenclature, we should use the term “right atrioventricular valve”, but we deliberately continue to use the term “tricuspid valve”.

⁸A septal defect situated in this posterior part of the membranous septum or interatrioventricular portion is responsible for a left ventricle-right atrium communication.

⁹This difference of thickness (and size), less marked at birth due to the fetal “balanced” right-left circulation, gradually increases, so that the heart progressively takes on the appearance of an “adult” heart with a dominant “systemic” left ventricle.

¹⁰Here again, according to the new nomenclature, we should use the term “left atrioventricular valve”, but we deliberately continue to use the term “mitral valve”.

Criteria for identification of the left ventricle are therefore:

- The mitral valve always opens into the left ventricle; it is identified by its more posterior position compared to the septal insertion of the tricuspid valve (offset of the valves depicted in “four-chamber long-axis” images and axial images (Fig. 2.7 and atlas A9, 10)).
- The presence of “mitro-aortic” continuity between the aortic and mitral rings (Fig. 2.8, atlas A8, S2).
- The presence of two papillary muscles (anterolateral and posteromedian) inserted onto the free wall (short-axis image (Fig. 2.3h)).

2.6.5 Pulmonary Artery

The pulmonary artery trunk¹¹ normally arises from the right ventricle, at the pulmonary orifice (comprising three semilunar cusps) at the summit of the infundibulum (conus), situated to the left and anteriorly to the aorta (atlas A6): it travels posteriorly, to the left and slightly superiorly and rolls around the left anterior surface of the ascending aorta forming a curve with a right posterior concavity (Figs. 2.4 and 2.9). Behind the left margin of the aorta, it divides into the left pulmonary artery continuous with the trunk, situated in an almost sagittal plane (atlas A4 and S4) crossing the left main bronchus almost perpendicularly by forming an arch with a superolateral convexity over the bronchus (Figs. 2.4 and 2.9), and the right pulmonary artery (larger and longer than the left pulmonary artery), situated in a coronal plane (atlas A6 and F8) in front of the right main bronchus. The ligamentum arteriosum (remnant of the fetal circulation) arises from the superior edge of the pulmonary artery and joins the descending aorta close to its origin (normally, the ductus arteriosus rapidly involutes at birth).

The criteria for identification of the pulmonary artery are:

- Bifurcation into left and right pulmonary arteries (Fig. 2.9 and atlas A4–6, F8, 9).
- Discontinuity between the tricuspid and pulmonary rings, in the normal configuration, due to the presence of the subpulmonary conus arteriosus (see morphologically right ventricle).

¹¹The diameter of the PA at its origin in adults is normally equal to 0.85 times that of the aorta.

2.6.6 Aorta

The aorta normally emerges from the left ventricle in a “central,” posterior and right position (compared to the pulmonary artery). It has an ascending portion first, and then a horizontal portion, usually describing a left-sided arch over the pulmonary artery trunk (Fig. 2.4). It is situated in a vertical plane, oblique anteroposteriorly and from right to left (LAO, Fig. 2.8). The ascending portion, almost entirely intrapericardial, contains the aortic orifice with three semilunar valves: one posterior (noncoronary), and the other two right and left anterolateral giving rise to coronary arteries. The horizontal segment gives rise to three arteries: brachiocephalic trunk anterior to the trachea, left common carotid artery lateral to the trachea, and left subclavian artery lateral to the esophagus. The isthmus of the aorta, situated at the origin of the descending aorta, is located between the origin of the left subclavian artery and the insertion of the ligamentum arteriosum.

The criteria for identification of the aorta are:

- Absence of division and the origin of supra-aortic vessels (Fig. 2.8).
- Origin of the coronary artery (both coronary sinuses are always situated over the pulmonary artery regardless of the aorta/pulmonary artery arrangement).
- “Mitro-aortic” continuity between the posterior part of the aortic root (posterior semilunar cusp) and the anterior leaflet of the mitral valve¹¹.

2.7 Atlas of Normal MR Anatomy of the Heart and Mediastinum

The following atlas is numbered in the direction of blood flow for cardiac chambers and great vessels. Numbering arbitrarily starts at the right atrium (1). The right ventricle is therefore number 2, the pulmonary artery is number 3, the pulmonary veins are number 4 etc. Names in bold type correspond to the new nomenclature (the old nomenclature is sometimes indicated in parentheses). Names with capital letters correspond to abbreviations used in the diagrams and some of the figures in this book.

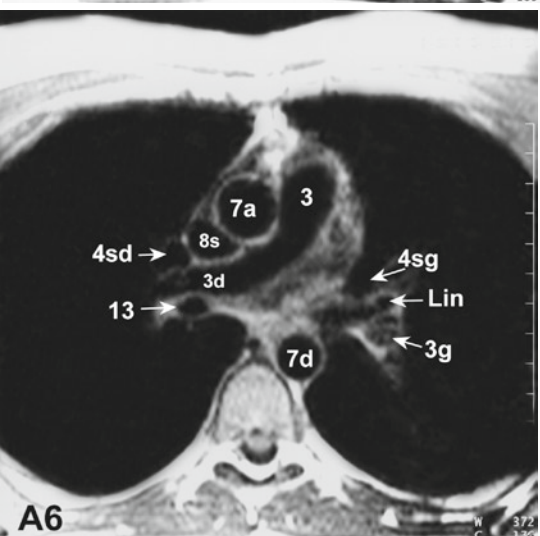
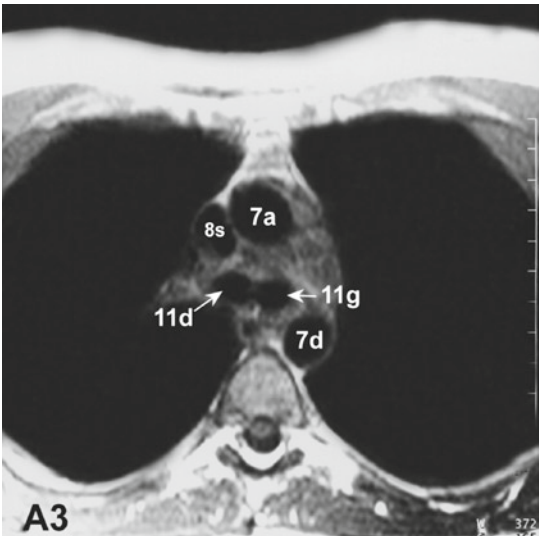
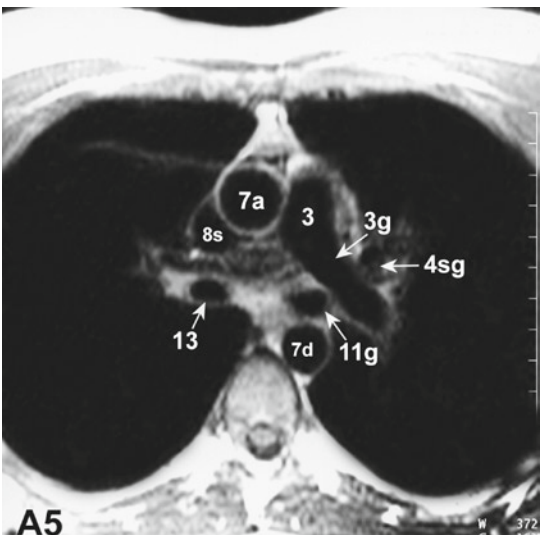
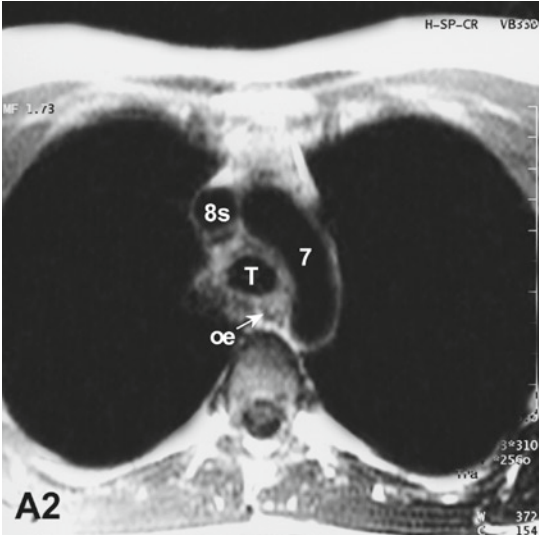
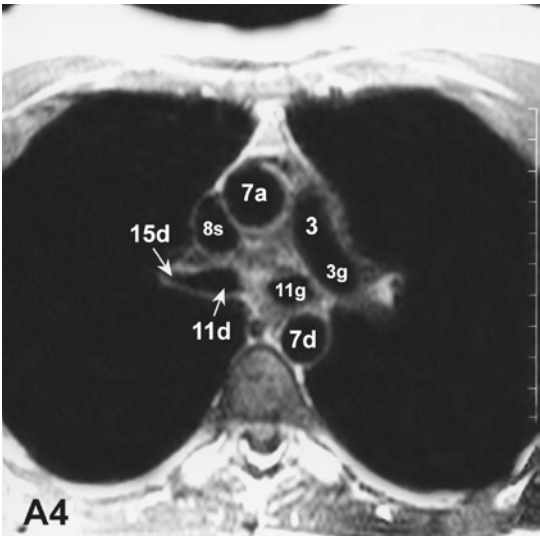
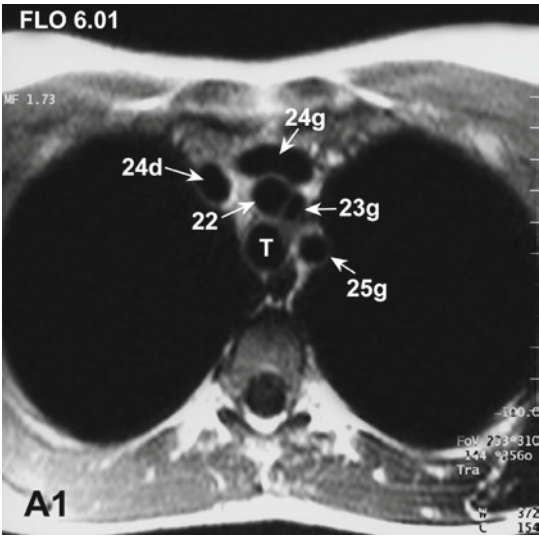
Images were acquired by various spin-echo or fast spin-echo black-blood techniques.

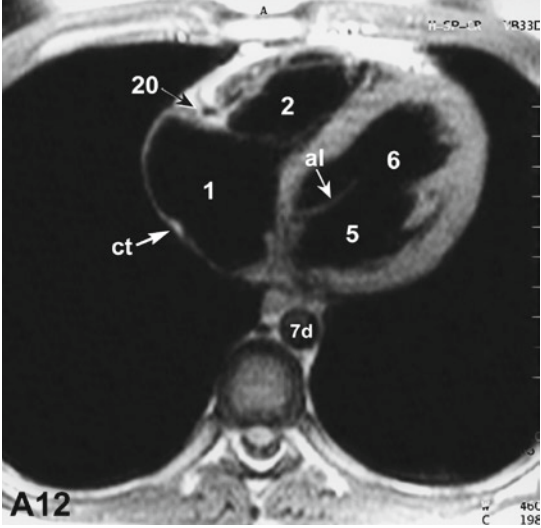
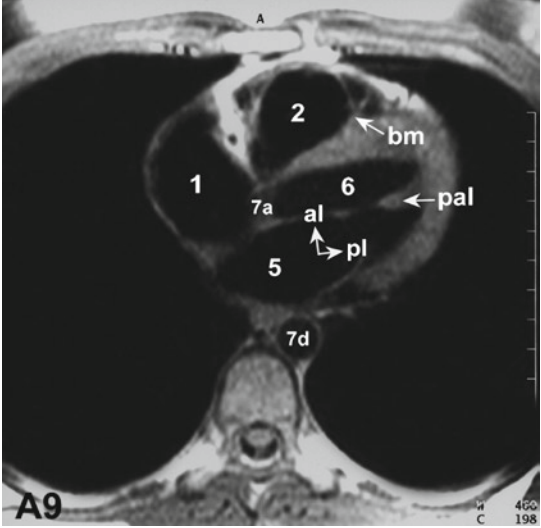
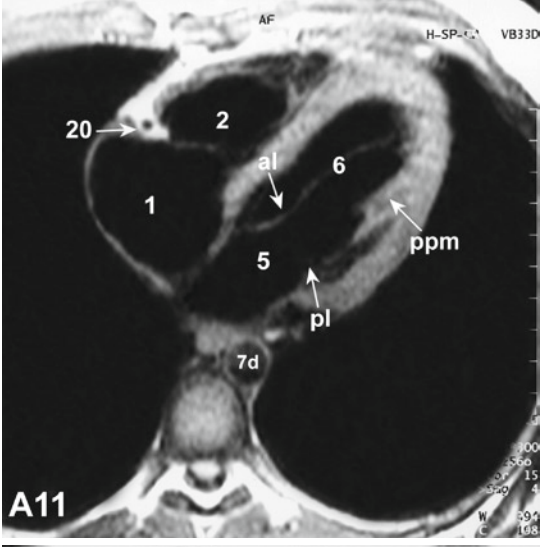
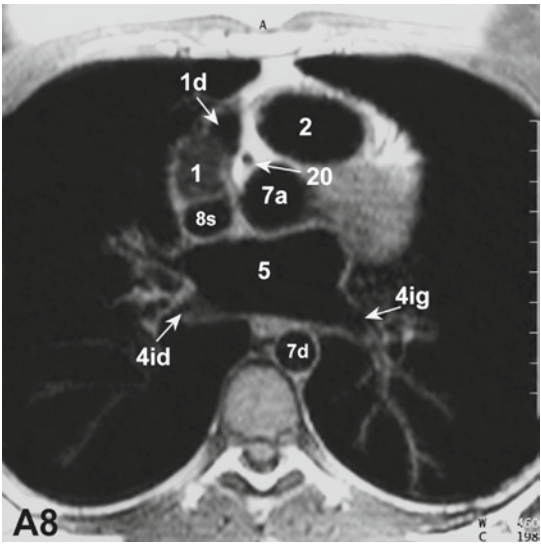
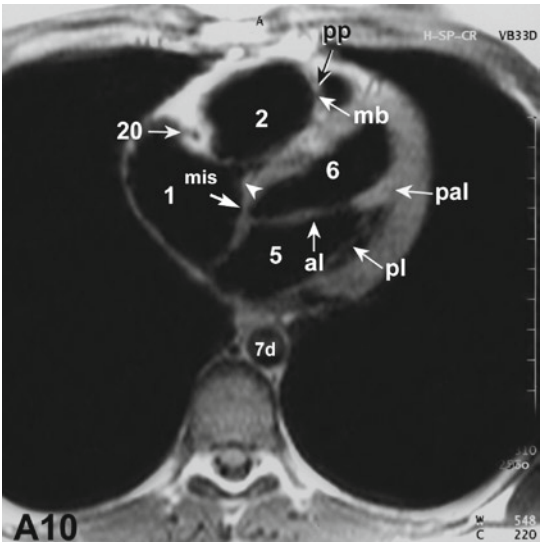
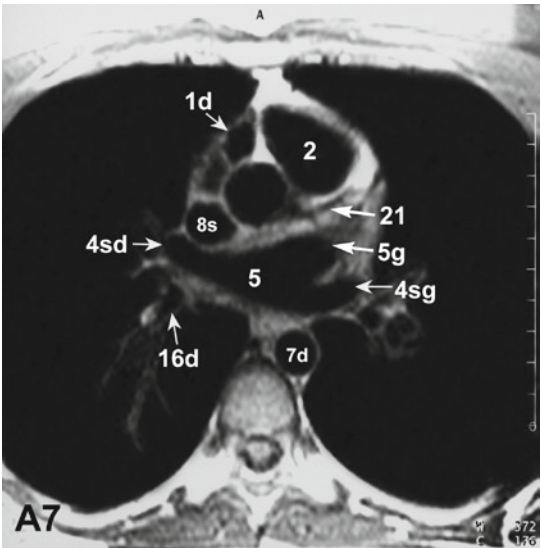
- A1–15: Craniocaudal series of axial images (fast spin-echo segmented with cardiac gating, slice thickness: 5 mm).

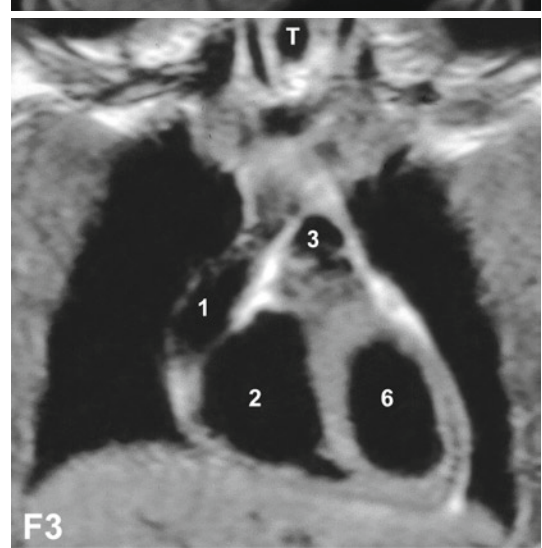
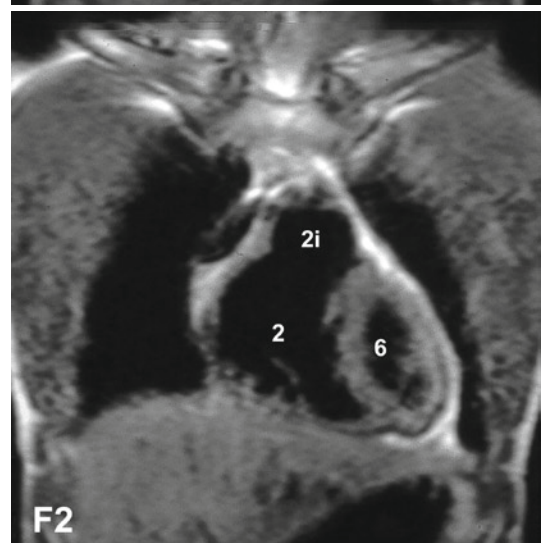
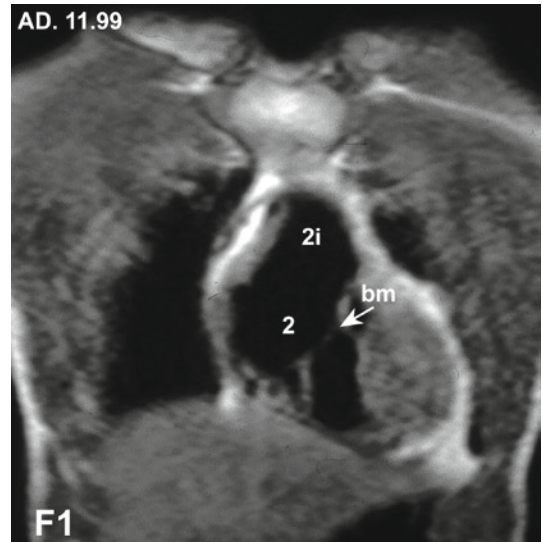
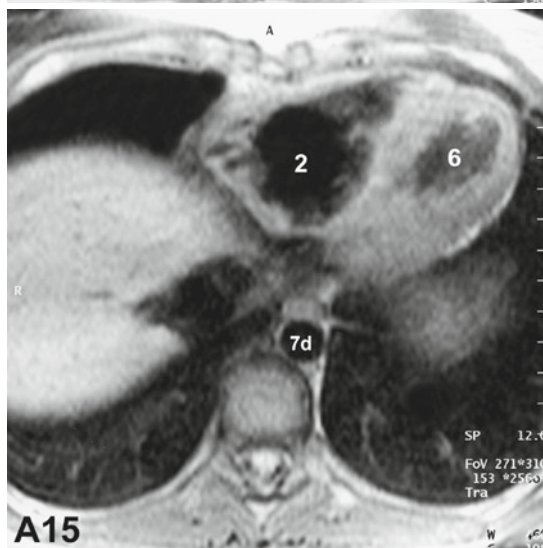
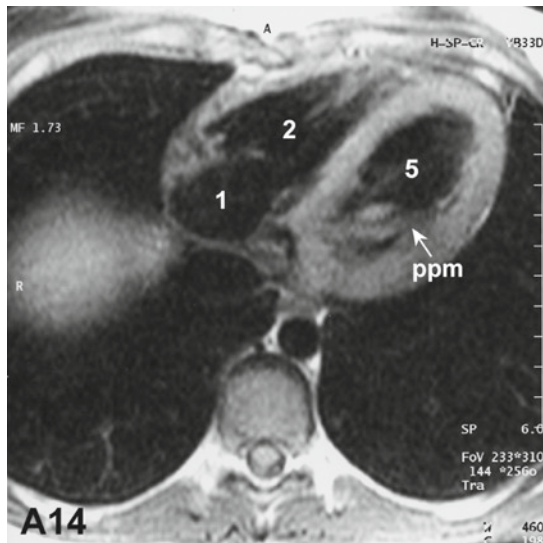
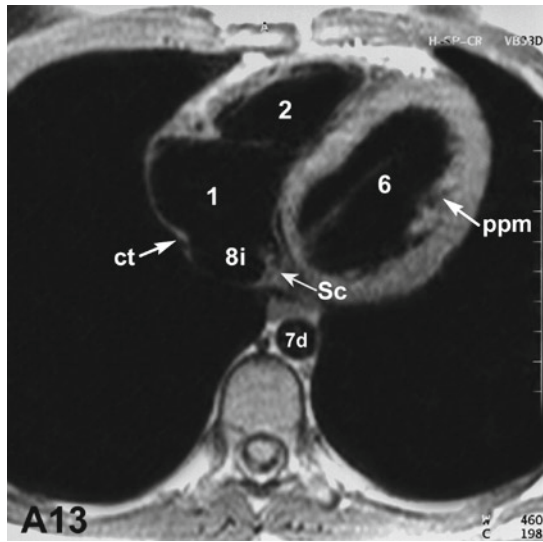
- F1–14: Anteroposterior series of coronal images (ECG-gated spin-echo, slice thickness: 7 mm).
- S1–7: Sagittal images from right to left (half-Fourier ECG-gated fast spin-echo, slice thickness: 7 mm).

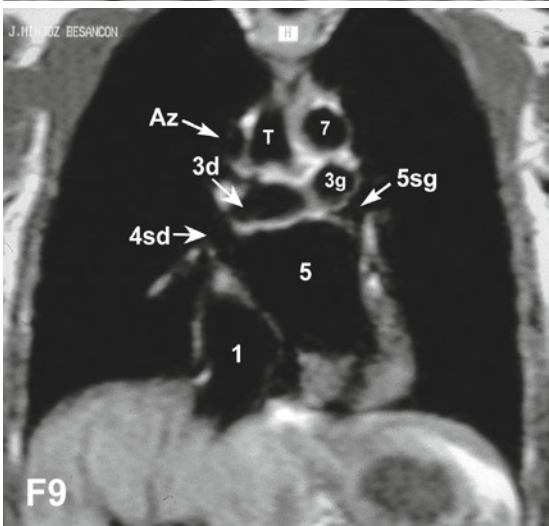
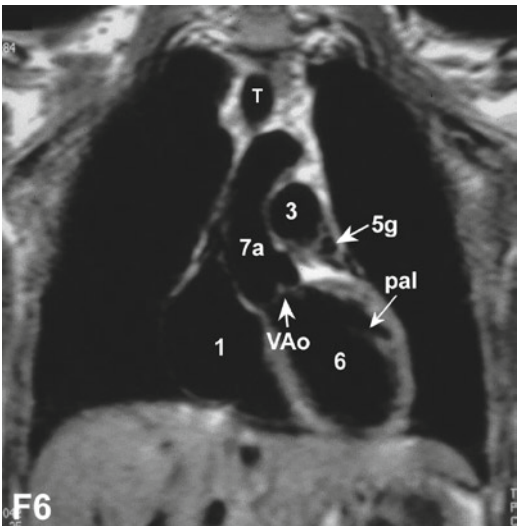
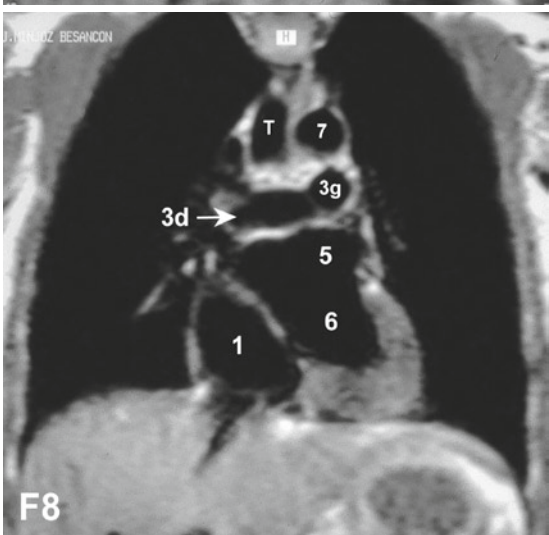
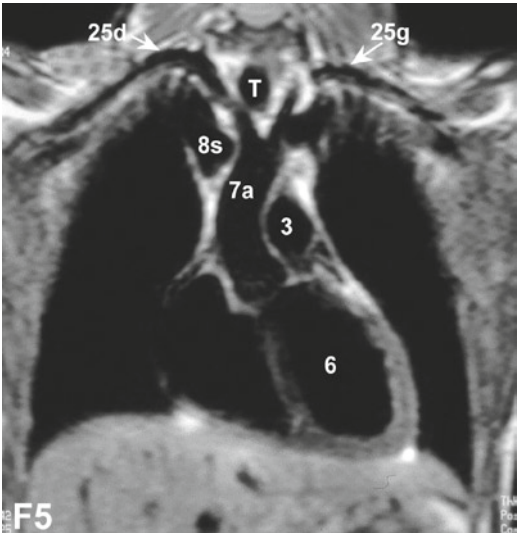
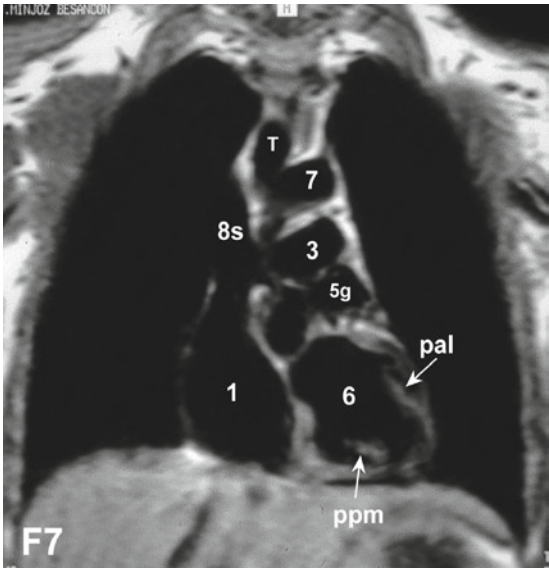
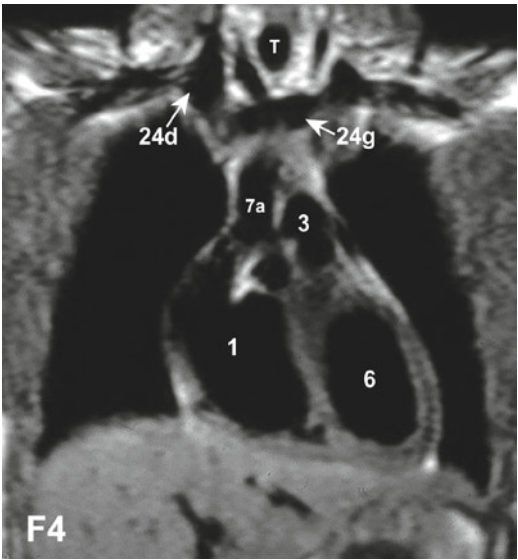
1	right atrium RA
1'	morphologically right atrium situated on the left
1d	right atrial appendage RAa
2	right ventricle RV
2'	morphologically right ventricle RV situated on the left
pp	main papillary muscle
mb	moderator band (septomarginal trabecula)
2i	pulmonary infundibulum
3	pulmonary artery trunk PA, pulmonary valve PuV
3d	right pulmonary artery RPA
3g	left pulmonary artery LPA
4	pulmonary vein PV
4sd	right superior pulmonary vein
4sg	left superior pulmonary vein
4id	right inferior pulmonary vein
4ig	left inferior pulmonary vein
5	left atrium LA
5'	morphologically left atrium situated on the right
5g	left atrial appendage LAa
6	left ventricle LV
6'	morphologically left ventricle situated on the right
pal	anterolateral papillary muscle
ppm	posteromedian papillary muscle
7	aorta Ao
7a	ascending aorta AAo
7d	descending thoracic aorta Dao
7i	abdominal aorta AbdAo
8 s	superior vena cava SVC
8sd	right superior vena cava RSVC
8sg	left superior vena cava LSVC
8i	inferior vena cava IVC
T 9	Trachea
10	Esophagus
Th	Thymus

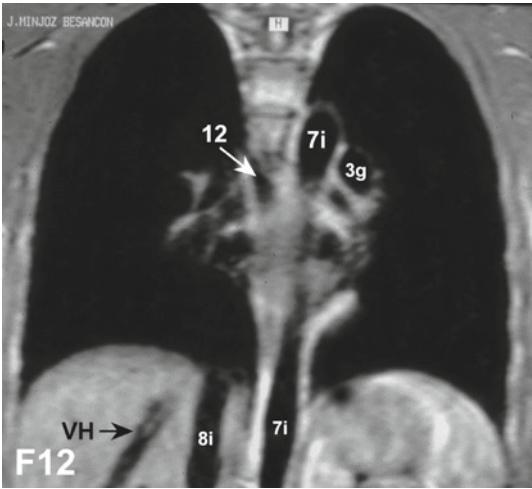
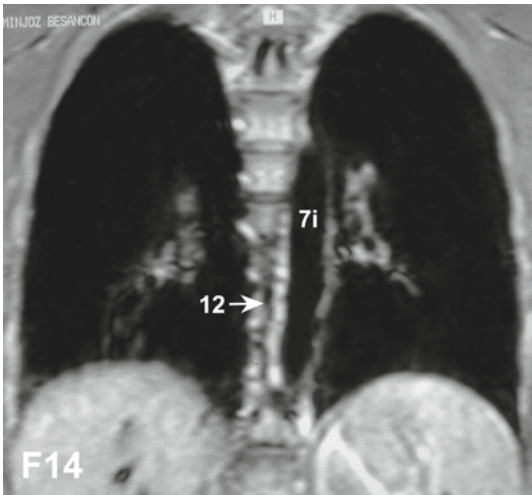
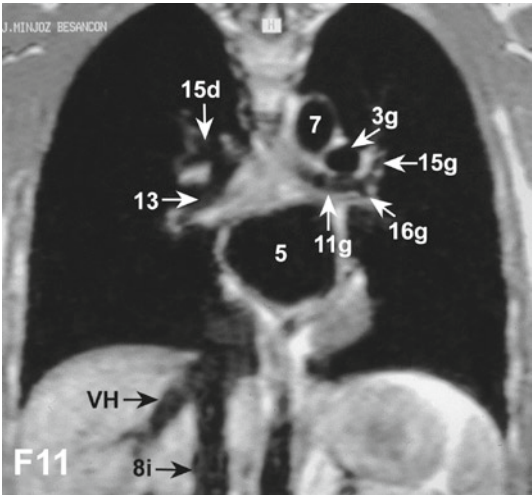
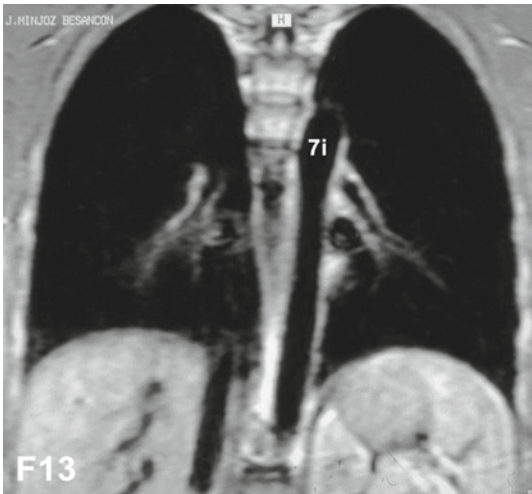
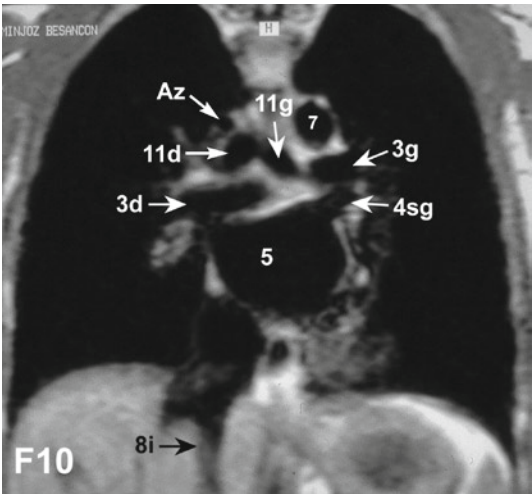
11d	right main bronchus R
11g	left main bronchus L
12, 12d	azygos vein AzV
12g	(left) hemiazygos vein (superior or inferior)
13	Bronchus intermedius
14	lower lobe artery (14d-right, 14g-left)
15	lobar bronchus (right upper lobe-15d, middle lobe-15m, left upper lobe-15g)
16	lower lobe bronchus (right-16d, left-16g)
17	superior pericardial recess
18	circumflex artery
19	left anterior descending artery
20	right coronary artery RCo
Tc	left coronary artery trunk
21	left coronary artery LCo
cs	coronary sinus
VM or M	left atrioventricular valve (mitral -bicuspid-valve) (arrow), Gv
MV or M	anterior leaflet,
TV or T	pv posterior leaflet
VT or T	right atrioventricular valve (tricuspid valve) (arrowhead)
VAo	aortic valve
PuV	pulmonary valve
22	brachiocephalic trunk (innominate artery)
23d	right common carotid artery RC
23g	left common carotid artery LC
24d	right brachiocephalic vein (right innominate vein) RBCV
24g	left brachiocephalic vein (left innominate vein) LBCV
Mi	internal mammary artery (internal thoracic artery)
25d	right subclavian artery RSC
25g	left subclavian artery LSC
26i	posterior mitral papillary muscle (inferior papillary muscle of left ventricle)
27	mediastinal trunk (s) (right superior mediastinal artery)
ct	crista terminalis
Lin	lingular bronchus
HV	hepatic veins
VR	renal veins
PV	portal vein

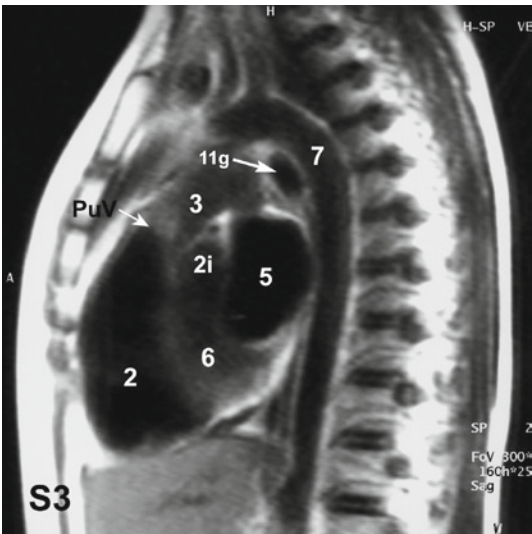
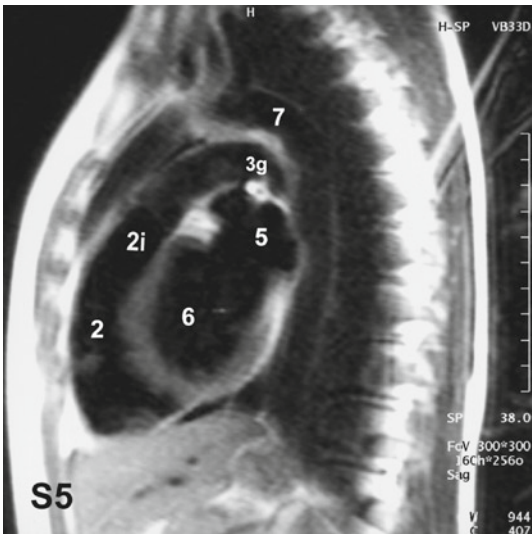
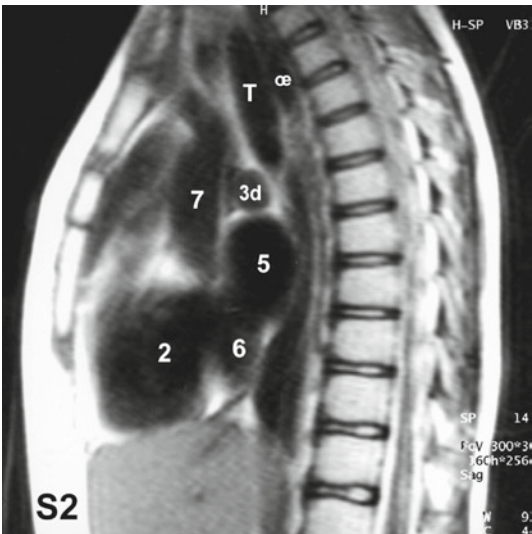
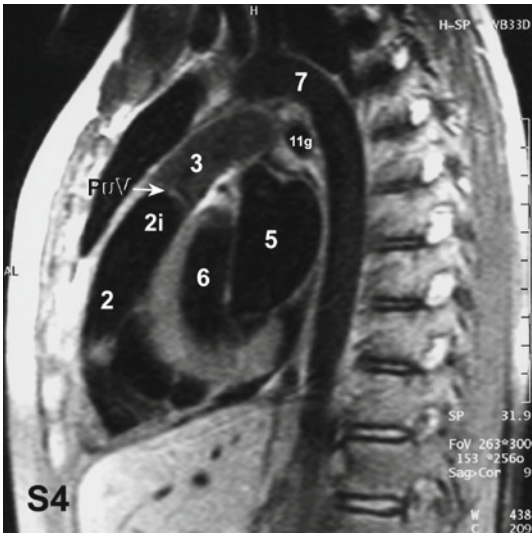
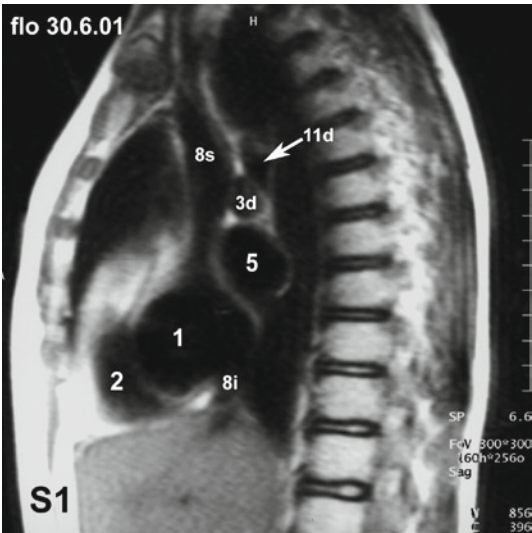


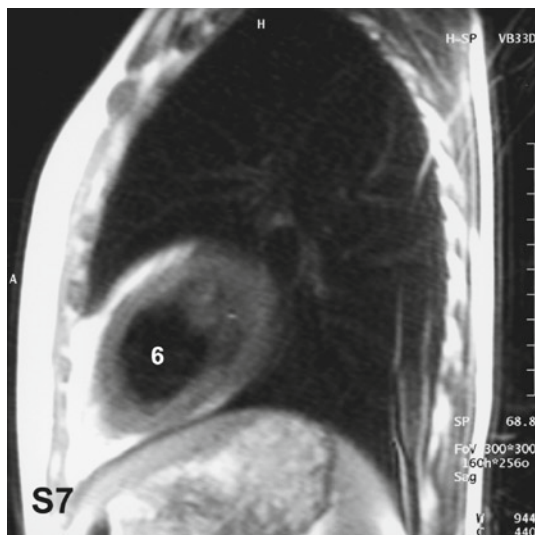












References

1. Fletcher BD, Jacobstein MD, Nelson AD, et al. Gated MRI of congenital cardiac malformation. *Radiology*. 1984;150:137–40.
2. Higgins CB, Byrd BF, Farmer DW, et al. MRI in patients with congenital heart disease. *Circulation*. 1984;70:851–60.
3. Jacobstein MD, Fletcher BD, Nelson AD, Goldstein S, Alfidi RJ, Riemenschneider TA. ECG-gated nuclear magnetic resonance imaging: appearance of the congenitally malformed heart. *Am Heart J*. 1984;107:1014–20.
4. Higgins CB, Byrd BF, McNamara MT, et al. Magnetic resonance imaging of the heart: a review of the experience in 172 subjects. *Radiology*. 1985;155:671–9.
5. Fletcher BD, Jacobstein MD. MRI of congenital abnormalities of the great vessels. *AJR*. 1986;146:941–8.
6. Didier D, Higgins CB, Fisher MR, et al. Gated MRI in congenital heart disease: initial experience in 72 patients. *Radiology*. 1986;158:227–35.
7. Boxer RA, Singh S, La Corte MA, et al. Cardiac MRI in children with congenital heart disease. *J Pediatr*. 1986;109:460–4.
8. Gomes AS, Lois JF, George B, Alpan G, Williams RG. Congenital abnormalities of the aortic arch. *Radiology*. 1987;165:691–5.
9. Chung KJ, Simpson IA, Newman R, et al. Cine-MRI for evaluation of congenital heart disease: role in pediatric cardiology compared with echocardiography and angiography. *J Pediatr*. 1988;113:1028–35.
10. Sieverding L, Klose U, Aplitz J. Morphological diagnosis of congenital and acquired heart disease by MRI. *Pediatr Radiol*. 1990;20:311–9.
11. Parson JM, Baker EJ, Hayes A, et al. MRI of the great arteries in infants. *Int J Cardiol*. 1990;28:73–85.
12. Bank ER. Magnetic resonance of congenital cardiovascular disease: an update. *Radiol Clin North Am*. 1993;31:553–72.
13. Kastler B, Livolsi A, Germain P, et al. MRI in congenital heart disease of newborns. Preliminary results in 23 patients. *Eur J Radiol*. 1990;10:109–17.
14. Livolsi A, Kastler B, Germain P, et al. Indication de l'imagerie par résonance magnétique dans les cardiopathies congénitales en période néonatale. *Ann Cardiol Angéiol*. 1991;40:129–33.
15. Kastler B, Livolsi A, Germain P, et al. MRI in the management of congenital heart disease in newborn and s. *Hospimedica*. 1991;9:31–41.
16. Guilt GI, et al. Levotransposition of the aorta: identification of segmental cardiac anatomy using MR imaging. *Radiology*. 1986;161:673–9.
17. Hagen PT, Schoz DG, Edward WD. Incidence and size of patent foramen ovale during the first 10 decades of live: an autopsy study of 965 normal hearts. *Proc Staff Meet Mayo Clin*. 1984;59:1489–94.
18. Soto B et al. Identification of thoracic isomerism from the plain chest radiograph. *AJR Am J Roentgenol*. 1978;131:995–1002.
19. Tonkin IL, Tonkin AK. Visceroatrial situs abnormalities: sonographic and computed tomographic appearance. *AJR Am J Roentgenol*. 1982;138:509–15.
20. Stanger P, Rudolph AM, Edwards JE. Cardiac malpositions: an overview based on a study of 65 necropsy specimens. *Circulation*. 1977;56:159–72.
21. Kastler B, Livolsi A, Germain P. Strip scanning a method to improve pediatric cardiovascular MRI. *SMRI, 9th Annual Meeting, Chicago, April 3–6, 1991. (JMRI)*.
22. Kastler B, et al. MRI Artifacts a comprehensive approach. *RSNA, 81th Assembly and Annual Meeting, Chicago, November 26–December 3, 1996. Artefacts en IRM. Feuilles de Radiologie* 1994;34(6):493–514.
23. von Schulthess GK, Higgins CB. Blood flow imaging with MR: spin-phase phenomena. *Radiology*. 1985;157:687–95.
24. Felmlee JP, Ehman RL. Spatial presaturation: a method for suppressing flow artifacts and improving depiction of vascular anatomy in MR imaging. *Radiology*. 1987;164:559–64.
25. Link KM, Lesko NM. Magnetic resonance imaging in the evaluation of congenital heart disease. *Magn Reson Q*. 1991;7:173–90.
26. Higgins CB, editor. *MRI of congenital heart disease. Essentials of cardiac radiology and imaging*. Philadelphia: Lippincott; 1992. p. 283–331.
27. Wehrli FW, Haacke EM. Principles of MR imaging. In: Potchen EJ, Haacke EM, Siebert JE, Gottschalk A, editors. *Magnetic resonance angiography: concepts and applications*. St Louis: Mosby-Year Book; 1993. p. 9–34.
28. Listerud J. First principles of magnetic resonance angiography. *Magn Reson Q*. 1991;7:136–70.
29. Kastler B, editor. *Dans: Comprendre l'IRM: Imagerie du flux*. 6th ed. Paris: Masson; 2006. p. 189–213.
30. Atkinson D, Teresi L. Magnetic resonance angiography. *Magn Reson Q* 1994;10:149–72.
31. von Schulthess GK, Fisher S, Crooks LE, et al. Gated MR imaging of the heart: intracardiac signals in patients and healthy subjects cardiac. *Radiology*. 1985;156(1):125–32.

32. Kastler B. Principles of MR angiography. In: Patay Z, Kastler B, Anzalone N, editors. *Applied neuroMR angiography CD-ROM*. Antwerpen: Lasion; 1996.
33. Sechtem U, Pflugfelder PW, White RD, et al. Cine MR imaging: potential for the evaluation of cardiovascular function. *AJR Am J Roentgenol*. 1987;148:239–46.
34. Sechtem U, Pflugfelder P, Cassidy MC, Holt W, Wolfe C, Higgins CB. Ventricular septal defect: visualization of shunt flow and determination of shunt size by cine MR imaging. *AJR Am J Roentgenol*. 1987;149:689–92.
35. Baker EJ, Ayton V, Smith MA, et al. Magnetic resonance imaging at a high field strength of ventricular septal defects in infants. *Br Heart J*. 1989;62:305–10.
36. Simpson IA, Chung KJ, Glass RF, Sahn DJ, Sherman FS, Hesselink J. Cine magnetic resonance imaging for evaluation of anatomy and flow relations in s and children with coarctation of the aorta. *Circulation*. 1988;78:142–8.
37. Edelman RR, Chien D, Kim D. Fast selective black blood MR imaging. *Radiology*. 1991;181(3):655–60.
38. Boisselle PM, White CS. New techniques in cardiothoracic imaging. New York: Informa Healthcare; 2007. p. 81–2.
39. Weber OM, Higgins CB. MR evaluation of cardiovascular physiology in congenital heart disease: flow and function. *J Cardiovasc Magn Reson*. 2006;8(4):607–17.
40. Rebergen SA, Niezen RA, Helbing WA, van der Wall EE, de Roos A. Cine gradient-echo MR imaging and MR velocity mapping in the evaluation of congenital heart disease. *Radiographics*. 1996;16(3):467–81.
41. Mostbeck GH, Caputo GR, Higgins CB. MR measurement of blood flow in the cardiovascular system. *AJR Am J Roentgenol*. 1992;159:453–61.
42. Nayler GL, Firmin DN, Longmore DB. Blood flow imaging by cine magnetic resonance. *J Comput Assist Tomogr*. 1986;10:715–22.
43. Bogren HG, Klipstein RH, Firmin DN, et al. Quantification of antegrade and retrograde blood flow in the human aorta by magnetic resonance velocity mapping. *Am Heart J*. 1989;117:1214–22.
44. Rees S, Firmin D, Mohiaddin R, Underwood R, Longmore D. Application of flow measurements by magnetic resonance velocity mapping to congenital heart disease. *Am J Cardiol*. 1989;64:953–6.
45. Pelc NJ, Herfkens RJ, Shimakawa A, Enzmann DR. Phase contrast cine magnetic resonance imaging. *Magn Reson Q*. 1991;7:229–54.
46. Kilner PJ, Firmin DN, Rees RSO, et al. Valve and great vessel stenosis: assessment with MR jet velocity mapping. *Radiology*. 1991;178:229–35.
47. Rebergen SA, Van Der Wall EE, Doornbos J, De Roos A. Magnetic resonance measurement of velocity and flow: technique, validation, and cardiovascular applications. *Am Heart J*. 1993;126:1439–56.
48. Pelc NJ, Sommer G, Li KCP, Brosnan TJ, Herfkens RJ, Enzmann DR. Quantitative magnetic resonance flow imaging. *Magn Reson Q*. 1994;10:125–47.
49. Carr JC, Simonetti O, Bundy J, Li D, Pereles S, Finn JP. Cine MR angiography of the heart with segmented true fast imaging with steady-state precession. *Radiology*. 2001;219(3):828–34.
50. Dinsmore RE, Wismer GL, Levine RA, Okada RD, Brady TJ. Magnetic resonance imaging of the heart: positioning and gradient angle selection for optimal imaging planes. *AJR Am J Roentgenol*. 1984;143:1135–42.



<http://www.springer.com/978-3-540-30701-3>

MRI of Cardiovascular Malformations

Kastler, B.

2011, XVII, 256 p., Hardcover

ISBN: 978-3-540-30701-3